Applied Catalysis B: Environmental 222 (2018) 18–25

Contents lists available at ScienceDirect

Applied Catalysis B: Environmental

journal homepage: www.elsevier.com/locate/apcatb

Research Paper

Evaluation of transferable TiO_2 nanotube membranes as electrocatalyst support for methanol photoelectrooxidation

J.A. Díaz-Real[a], G.C. Dubed-Bandomo[b], J. Galindo-de-la-Rosa[b], E. Ortiz-Ortega[b], J. Ledesma-García[a], L.G. Arriaga[b,*]

[a] Facultad de Ingeniería, División de Investigación y Posgrado, Universidad Autónoma de Querétaro, Centro Universitario Cerro de las Campanas, Querétaro, Qro., C.P. 76010, Mexico

[b] Centro de Investigación y Desarrollo Tecnológico en Electroquímica, Pedro Escobedo, Qro., C.P. 76703, Mexico

ARTICLE INFO

Keywords:
Transferable TiO_2 nanotube membrane
Energy generation
Photo-electrocatalytic activity
Flexible photoelectrode
Methanol oxidation

ABSTRACT

TiO_2 nanotube membranes (TNM) were synthesized, separated (by electrochemical anodization) and modified with Pt-Ru electrocatalyst to assess their photoelectrocatalytic activity towards methanol (MeOH) oxidation. The feasibility of use of these composite materials was evaluated in different supports to observe the development of the electrochemical responses as a function of the nature of the electrical collecting substrate. The results suggested that, while the Pt-Ru decorated TMN present photoelectrocatalytic activity, the electrical contact in the back might be the limiting step in current collection. Such findings were demonstrated by performing scanning electrochemical microscopy SECM over the surface of the TNMs, where methanol was oxidized in the microelectrode tip of the SECM. This approach corroborated the suitability of TNMs to be modified with an electrocatalyst and its application in current technology such as microfluidic fuel cells.

1. Introduction

Among the various nanomaterials, TiO_2 nanotubes (NTs) are regarded as one of the most promising candidates for energy and environmental applications holding great potential due to its innocuity, low-cost, enhanced surface hydrophilicity and excellent physical and chemical stability [1–3]. Their high photocatalytic activity of NTs results from their specific surface area, crystallinity and porous structure [4,5]. Due to its bandgap, NTs require UV light irradiation to generate photo-induced charge carriers (electron-hole pairs) and such characteristic has been used in several fields such as alternative energy technologies, photocatalysis, solar cells, gas sensing and photo-electrochemical cells [6]. To properly profit from the advantages of this morphology in photoelectrocatalytic applications, the substrate-electrode (S.E.) configuration should be used as it is the most efficient in such systems. However, the nature of the synthesis process of NTs prevents from using the S.E. configuration since they are strongly attached to the metallic Ti substrate which difficulty their assessment in this technology.

With the current surface engineering development, cutting-edge morphologies in the nanometer scale can be tailored for specific applications. As an electrocatalyst support, TiO_2 has been used in the electrodes for microfluidic fuel cells to improve the performance of noble metal electrocatalyst like Pt and Pd, by modifying the electronic surface properties [7–9]. Such cells have evolved to the point of producing flexible assemblies, thus the possibility of incorporating a flexible TiO_2 membrane (TNM) in these systems represents a promising alternative to design next-gen devices that can be adapted to complicated topologies, such as in textiles, on-skin sensors and medical applications [10–14].

However, to the best of our knowledge, the reports on the preparation of TNM modified with electrocatalytic materials are very scares; as a structured photoelectrocatalyst, to study its activity towards methanol electrooxidation. Therefore, in this work, we report the synthesis and characterization of transferable TNMs modified with Pt-Ru electrocatalyst; The photocatalytic activity towards methanol electrooxidation was evaluated under UV light by scanning electrochemical microscopy (SECM) technique to verify the photo-generated holes.

2. Experimental setup

2.1. Preparation of photocatalytic supports

2.1.1. Synthesis of TNM

The preparation technique for the TNM was performed by electrochemical anodization [15]. Metallic titanium sheets (99% purity,

* Corresponding author.
E-mail address: larriaga@cideteq.mx (L.G. Arriaga).

http://dx.doi.org/10.1016/j.apcatb.2017.09.019
Received 6 July 2017; Received in revised form 5 September 2017; Accepted 7 September 2017
Available online 28 September 2017
0926-3373/

thickness 0.127 mm, Alfa-Aesar) were sand-paper polished. Subsequently, they were sonicated for 15 min in ethanol, acetone (Sigma-Aldrich) and distilled water successively and then dried under nitrogen gas flow (99.999, Praxair). Once cleaned, they were immersed in an acrylic cell in a 0.1 M NH_4F ethylene-glycol (96% purity, Alfa-Aesar) based electrolyte with 2% w/w deionized water. A two-electrode arrangement was used, with a steel sheet as a counter-electrode and placed at 2.5 cm from the working electrode. The potential imposed (E_1) between both electrodes was 60 V (BK Precision model 9184) and NTs-TiO_2 were grown at different anodizing times (t_{a1}) of 0.5, 1, and 4 h.

To induce the crystallinity of the nanotubes to their phase with better electrical conduction properties (anatase), a heat treatment was applied in a muffle (Tube Furnace 21 100) for 2 h at 450 °C, with a temperature ramp of 10 °C/min under air atmosphere.

2.1.2. Detachment of TNM

The easy and complete detachment of nanotubes was achieved with the application of a second anodizing process after the heat treatment.

A potential of 160 V (E_2) for 30 s (t_{a2}) was imposed on all the anodes obtained at different times. After the NTs were embrittled, the anodized sheet was rinsed in EtOH and then in water for 15 min. Finally, with a slight mechanical stress it is possible to separate the membrane (See Fig. S1 in supplementary information).

2.1.3. Transfer of membranes on ITO glass

The transfer of the membranes was performed using ITO glass as a conductive substrate and Nafion (5 wt.% Sigma Aldrich) as an adhesive, aiming to approximate the system to the methods used in the fuel cells to evaluate the catalytic inks by the drop-cast technique, being a method little explored to achieve the electrical interconnection between the membrane and the conductive support, where contact is generally achieved using sintered TiO_2 nanoparticles, which subsequently require sintering to create adequate electrical continuity, the need to reach high temperatures to sinter the material precludes its application in substrates that are not thermally resistant. The membranes can be transferred to other conductive and flexible supports such as ITO/PET and an interesting alternative is how to develop transparent and flexible electrodes without the need for previous thermal treatments to achieve the interconnection between the membrane and the substrate conductor.

2.1.4. Deposition of Pt-Ru on TNM

The depositions of the materials achieved with Nafion (5 wt.% Sigma Aldrich) by the drop-cast technique. The ink composition had a ratio of 120 µl of isopropanol and 14 µl of Nafion per milligram of catalyst. The catalyst evaluated was Pt-Ru/XC-72 (Johnson Matthey, HiSPEC 5000) and 2 µl of ink was deposited.

2.2. Materials characterization

2.2.1. Physicochemical characterization of the electrodes

The morphology and microstructure of the samples were examined by Scanning Electron Microscope (SEM, JEOL/JSM-6510LV) equipped with a detector for dispersive energy spectroscopy (Bruker, XFlash 6I10). The elemental composition was analysed by an energy-dispersion spectroscopy (EDS, Oxford link system) analyzer, which was equipped to the SEM. X-ray Photoelectron Spectroscopy studies (XPS) studies allowed to complement the information of the elements present, of the chemistry, organization and morphology of the surface with a 3 Monocromatic Magics Thermo Scientifics, (model K-Alpha + Surface analysis). To confirm the identity of the formed film and corroborate the effectiveness of the heat treatment to induce crystallinity in them, Raman spectroscopy was performed with a Thermo Nicolet model DXR equipped with a 780 nm laser and a 12x optical microscope, the spectra were obtained with a power of 12 mW cm^{-2} and a grid aperture of the spectrophotometer of 50 µm. UV–vis diffuse reflectance spectra (DRS) of the samples were recorded on a UV–vis spectrophotometer (USB2 + F00099 Ocean Optics device), using Backscattering Probe, with a lamp of 180.50-880.52 nm. X-Ray Diffraction (XRD) pattern of the samples were recorded by X-ray diffraction spectrometer with Cu Kα radiation (D8-advance, Bruker-AXS, D8 Advance).

2.2.2. Photoelectrochemical characterization of TNM and TNM modified with Pt-Ru (Pt-Ru/TNM)

2.2.2.1. Cyclic voltammetry (CV), linear sweep voltammetry (LSV), chronoamperometry (CA). To study its electrochemical behaviour and photocatalytic activity towards methanol electrooxidation, an electrochemical cell (Fig. 6a) equipped with a quartz window was used.

Electrochemical measurements were performed on different media (0.5 M H_2SO_4 and 0.5 M MeOH/0.5 M H_2SO_4) bubbled with N_2 (99,999, Praxair) at room temperature using an experimental arrangement of three electrodes. In these experiments, the reference electrode and counter electrode were an Ag|AgCl and a graphite bar, respectively. The electrocatalytic properties to methanol oxidation were evaluated through CV with several sweeps between potentials of −0.35 to 0.8 V vs NHE at a scan rate of 50 mV s^{-1}. The LSV were performed in the same range of potentials as the CV but at 5 mV s^{-1}, while the CA were run at 0.2 V vs Ag|AgCl. The evaluation was performed under darkness and UV light, illuminating with a 365 nm LED lamp with an effective irradiation power (I_o) of 22.4 mW cm^{-2} at the working electrode distance.

2.3. Evaluation Pt-Ru/TNM by scanning electrochemical microscopy

The TNM was evaluated by this technique, using a scanning electrochemical microscope (Biologic, ac-SECM/SECM470, in SG/TC mode) and the images were obtained by means of the software MIRA. A four-electrode cell consisting in a graphite rod as auxiliary electrode, reference electrode of Ag|AgCl, a 25 µm diameter platinum ultramicroelectrode (UME) and a gold electrode (diameter: 5.3 mm) as working electrode using a 0.5 M methanol in 0.5 M H_2SO_4 electrolyte. 2 µl of Nafion were applied to the surface of working electrode to bind it onto the TiO_2 membrane. The membrane was modified with an ink consisting of Pt-Ru/XC-72 (Johnson Matthey, HiSPEC 5000) dispersed in a solution isopropyl alcohol-water (1:3 ratio), and 14 µl of Nafion per mg by drop-cast deposition. Substrate generation and tip collection (SG/TC) mode of SECM was used, applying a potential of 0.2 V Ag|AgCl in the membrane, where the oxidation of methanol starts and 0.6 V vs Ag|AgCl in the platinum electrode for the oxidation of the generated formic acid.

3. Results and discussion

3.1. Physicochemical characterization TNM

The yellow coloration of the membrane increased with anodizing time and becomes more intense, which is associated with a greater incorporation of fluorides, but still allows the passage of light with ease (Fig. 1a–c). In Fig. 1, the SEM images also show well-defined NTs-TiO_2 arrangements with a regular and ordered structure over the entire anodized area. These structures had an average outer diameter of 84 nm and the total length of the nanotubes varies depending on the applied anodizing time (t_{a1}), obtaining nanotubes of 5, 13 and 31 µm in length for 0.5, 1 and 4 h respectively.

The samples produced with t_{a1} = 4 h evidenced the presence of a light layer on top of the nanotubes. At this condition, the lower concentration of water changes the stoichiometric conditions giving rise to Ti complexes that precipitate on the surface, both conditions being direct consequences of an increase in anodizing time. The water content in the organic electrolyte is a necessary parameter since it requires O^{2-} and H^+ for the growth and dissolution of the nanotubes and these ions come from water. The presence of this layer of precipitates on the

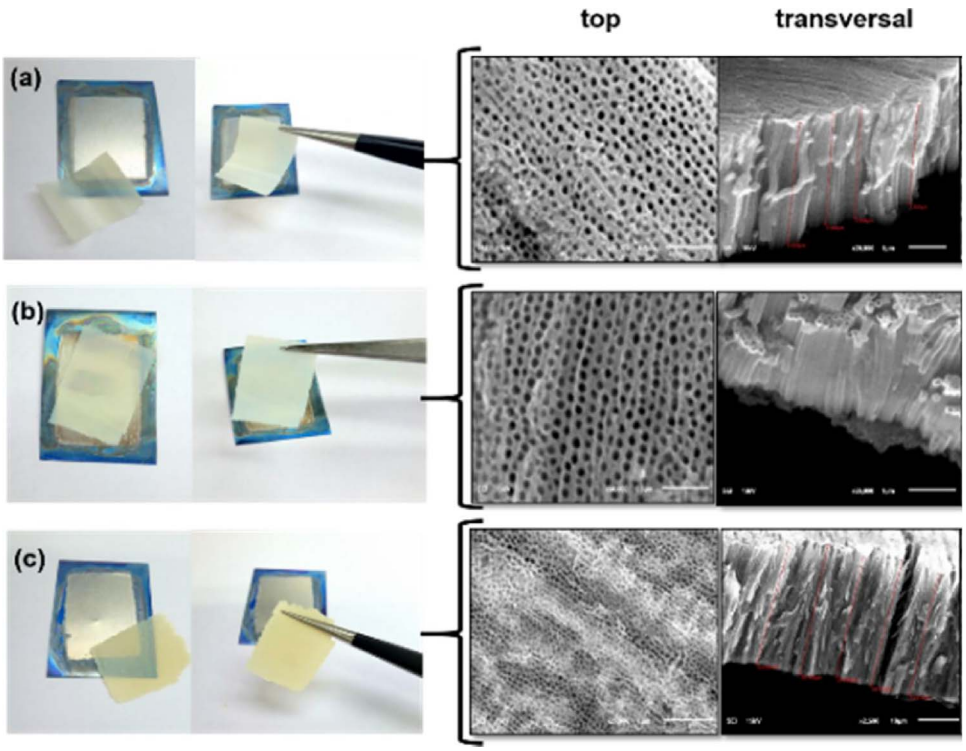

Fig. 1. Images of the TNM with different anodizing times (t_{a1}) of a) 0.5 h, b) 1 h, and c) 4 h respectively. At right show the top and transverse SEM images respectively.

surface of the nanostructures decreases the active area of the nanostructures as well as their morphological quality, which results in the loss of conductivity and therefore affects the functionality of the associated electrochemical processes [16].

Raman spectroscopy (Fig. 2) confirms the effect of the heat treatment on the crystallinity of the all membranes obtained at different anodizing times. Here we observe that anatase occurs as the dominant phase, with characteristic bands at 635, 514, 396 and 197 cm^{-1}, and a very intense and acute peak at 144 cm^{-1}. Rutile phase peaks are not observed [17]. No differences between the samples are observed but the intensity of the signals due to the length of the TNM.

XPS measurements were performed to study the surface composition and chemical states of the membranes and the acquired spectra are shown in Fig. 3. Regarding to the Ti positions (Fig. 3a), the distance of peaks between Ti $2p^1$ and Ti $2p^3$ is 5.6 eV, which means that the chemical state of the titanium is Ti^{4+} (TiO_2). There is an interesting difference observed in the sample with t_{a1} = 1.0 h, since the individual peaks of Ti $2p^1$ at 463 eV and Ti $2p^3$ at 458 eV are shifted compared to the 459.1 and 464.8 eV where are typically expected [18]. The small shift of Ti 2p peak due to the change of local chemical state of Ti ions influenced by N incorporation and Ti−N−O bond formation.

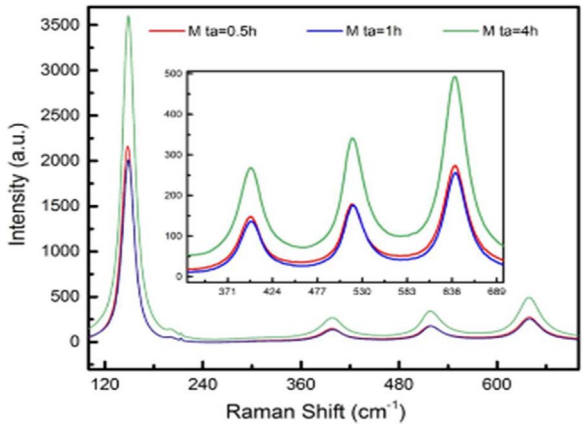

Fig. 2. Raman spectroscopy of the membranes.

As shown in Fig. 3b, for O 1s, the XPS peak is asymmetric for all conditions, which results from the contribution of two different environments. The main contribution, is attributed to lattice oxygen Ti−O, and the other contribution is ascribed to oxygen in surface hydroxyl groups or water (O−H bonding) [19]. These results confirm the existence of hydroxyl (OH^-) on the TiO_2 surface which can facilitate the photocatalytic properties of TiO_2 nanotube arrays. The Ti 2p and O 1s peaks of TNM samples are slightly shifted toward lower binding energy. The shifts of Ti 2p3/2 and the O 1s peaks are due to the introduction of oxygen vacancies into the TiO_2 lattice given by the incorporation of N atom into the TiO_2 lattice.

The spectra for F 1s is shown in Fig. 3c, where the peak is centered at 683.7 eV and is ascribed to the formation of metal fluorides (≡Ti−F) [20]. It is also clear the higher intensity for sample t_{a1} = 4.0 h which also showed a more yellowish colour (Fig. S1-a) due to a higher F incorporation. XPS attested that fluoride ions strongly adsorb on TiO_2, through an inner-sphere ligand substitution reaction with surface hydroxyl groups, as indicated by Eq. (1).

$$\equiv Ti{-}OH + F^- \leftrightarrow \equiv Ti{-}F + OH^- \quad (1)$$

This peak corresponds to surface fluorine formed by ligand exchange between fluoride anions in solution and surface hydroxyl groups at TiO_2 (TiOH), which is evidenced by the decrease of the asymmetric signal for the deconvolution of the O 1s.

Deconvolution of the N 1s peak (Fig. 3d) revealed the presence of two peaks with binding energy at 400 and 402 eV. As shown by Jagadale and co-workers' research [21], they indicated that the peak of N 1s located ranging from 398.8 to 400.8 eV belonged to electron binding energy of Ti−N−O and to anionic N incorporated in TiO_2 in O−Ti−N bonds. Also in this interval, it can be attributed to the presence of oxidized nitrogen such as N−O−Ti from the previous reports [22]. N doping also promotes the presence of OH surface. Therefore, the XPS results indicated that two forms of O−Ti−N and N−O-Ti coexist in doped TiO_2 nanotube array films, and is reported that the doping is substitutional and interstitial [19]. Both of these observations in XPS

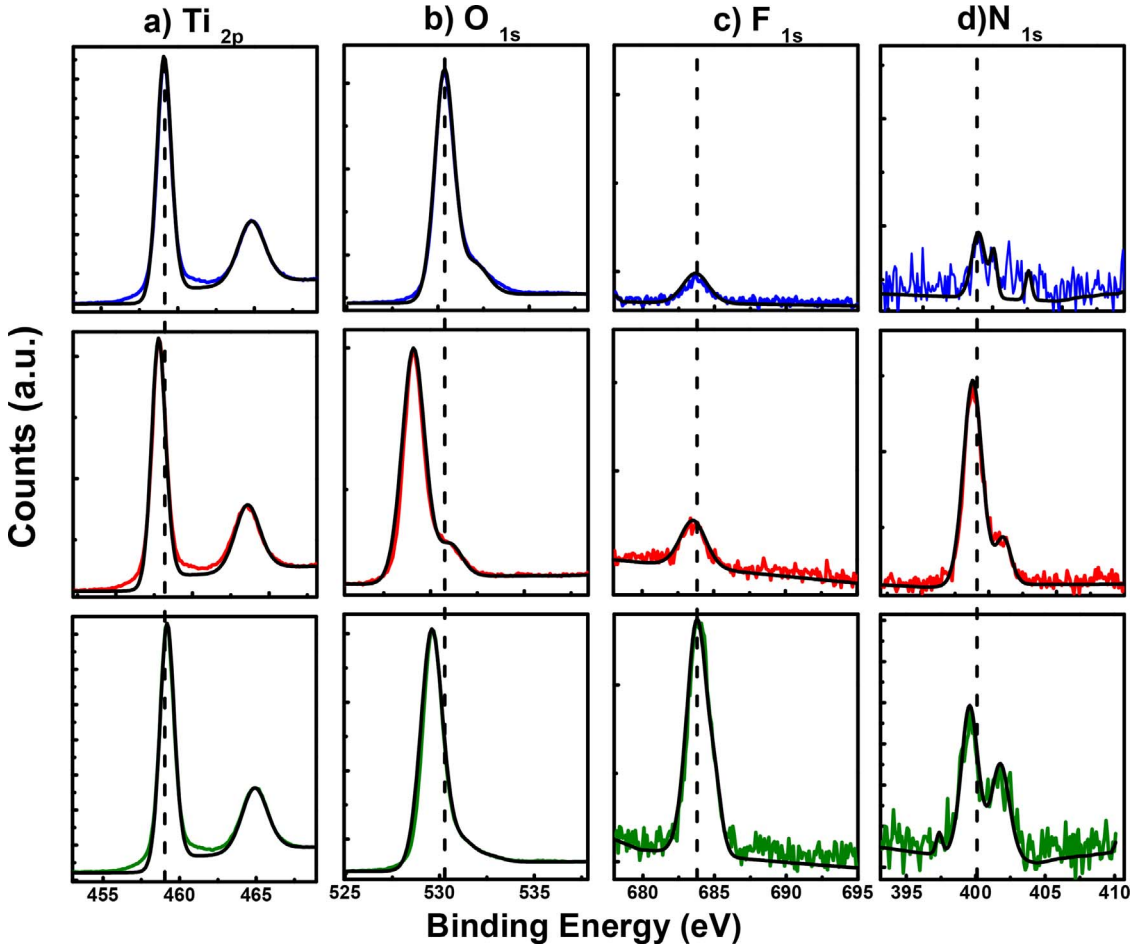

Fig. 3. XPS spectra of TNM with different anodizing times for a) Ti 2p, b) O 1s, c) F 1s and d) N 1s.

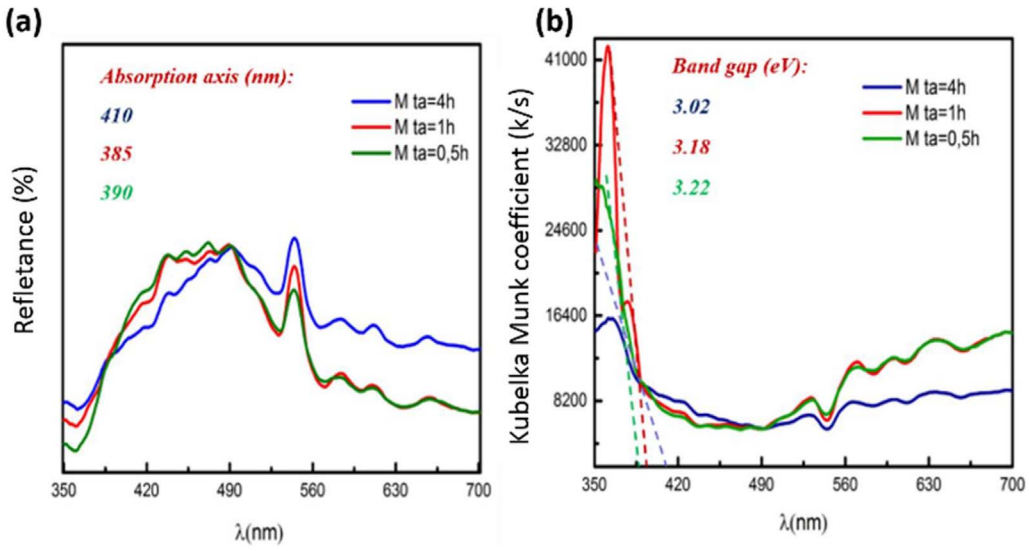

Fig. 4. (a) UV–vis diffuse reflectance (b) Kubelka Munk coefficient representation.

results are indicative that F + N co-doping is present and accompanied by oxygen vacancy formation.

Diffuse reflectance studies (Fig. 4a) were performed on the TNM to evaluate the light absorption response in the UV–vis spectrum with the modification of the composition of the membranes at different anodizing times. With the increase of the anodizing time an absorption edge shift occurs towards greater wavelengths. This displacement increases with the greater incorporation of F to reach until approximately 410 nm for the membrane corresponding to t_{a1} = 4 h. The phenomenon is translated on a macroscopic scale into the colour of the samples. The doped samples are yellow in colour, due to the absorption of visible radiation between 400 nm and 500 nm corresponding to the violet and blue colour in the light spectrum.

Yu and coworkers also observed that F-doping in TiO_2 powders had positive contribution in the reduction of the band gap as well as red shift in the absorption edge [23]. This observation becomes clearer in

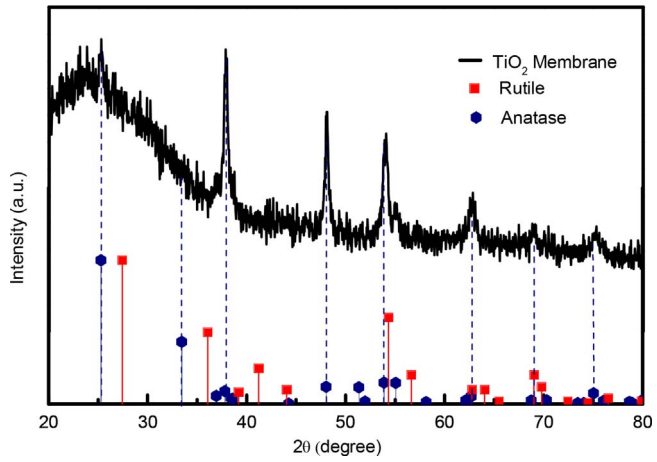

Fig. 5. X-ray diffractogram of TNM with t_{a1} = 1 h with glancing-angle configuration.

the Kubelka Munk coefficient representation (Fig. 4b) from which the band gap can be obtained by using the relation

$$E_g = \frac{1240}{\lambda_{Eg}} \quad (2)$$

Where λ_{Eg} (nm) is the absorption edge and E_g (eV) is the band gap [24]. It can be observed that the band gap obtained for the less doped sample is 3.22 eV, while the TNM with t_{a1} = 1 h presents a band gap of 3.18 eV, which is higher than t_{a1} = 4 h but with greater intensity of absorption. The latter might be due to a greater incorporation of ß-N that forms electronic states in the band gap very close to the valence band as confirmed by the studies of XPS [25]. Nevertheless, the higher content of F in our samples seem to drive the red shift in the absorption spectra, in agreement with the observations of Yu et al. [23].

The presence of vacancies of O can lead to the creation of electronic states located within the band gap near the conduction band that contribute to the decrease of the band gap. In fact, Rumaiz et al. [26] proposes that the sole presence of N-substitution cannot explain the decrease in band gap observed in the layers of N-doped TiO_2 and that it is the combination of N-substitution with O vacancies that explain the band gap reduction. In this regard, the O vacancies can also account from the F doping, attested in the XPS data.

We can conclude that the samples doped with nitrogen have photocatalytic activity under visible light due to the activation of the states present near the valence band associated to the N-substitution effect. For this reason, it was decided to use for the photoelectrocatalytic studies the membranes corresponding to t_{a1} = 1 h due to a greater absorption around the 385 nm.

The crystallinity of TNM (t_{a1} = 1 h) also was corroborated by XRD (Fig. 5) where the diffractogram confirms that the crystalline phase present is anatase and shows a very interesting preferential orientation for the crystalline plane (0 0 4) at 2Θ = 37.8°, which has been reported as an important photo-active plane [27].

In addition, the principal peak for anatase corresponding to the plane (1 0 1) (associated with reduction sites) at 25.3° does not match in relative intensity for the diffractogram obtained for this sample, since the peak having one greater intensity is that which appears in the 37.79° position and is characteristic of the plane (0 0 4). It is reported in the literature that this plane presents a higher photocatalytic activity and its growth is promoted under certain conditions of heat treatment and synthesis, in terms of heating rate, maximum temperature and anodizing time [28].

On the other hand, no other peaks corresponding to other crystalline phases were found than that of anatase. It should be noted that the sample analysed was a membrane detached from its metal substrate and that, as already mentioned, may have certain influence causing an apparent amorphicity observed as a broad shoulder between 20° and 35°

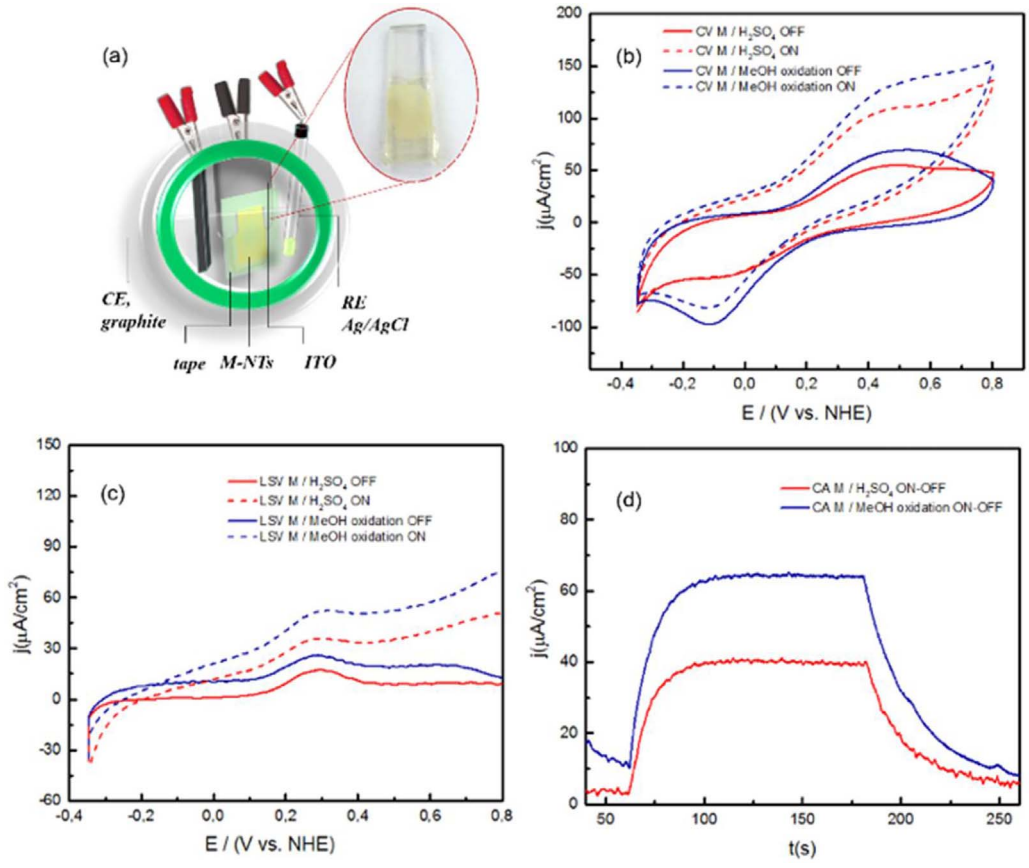

Fig. 6. (a) Scheme of the electrochemical cell, (b) cyclic voltammogram, (c) line sweep voltammograms and (d) chronoamperogram, all in 0.5 M H_2SO_4 and 0.5 M MeOH/0.5 M H_2SO_4.

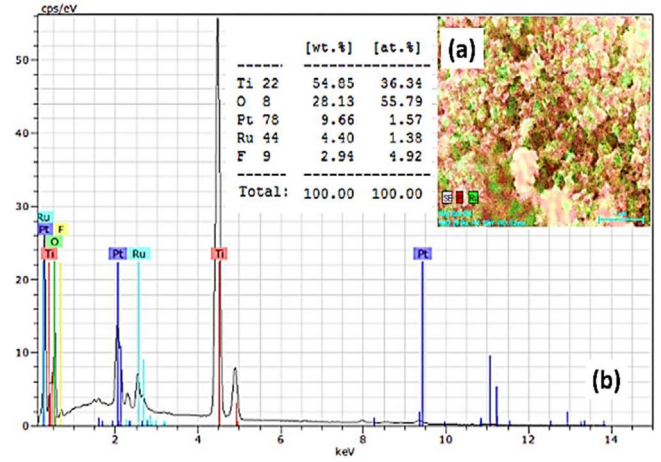

Fig. 7. a) SEM images when mapping the surface of Pt-Ru/TNM and b) EDS analysis of the electrode Pt-Ru/TNM.

of 2θ, especially as glancing-angle configuration was used. From the XRD diffractogram, the crystallite size was calculated by Debye-Scherrer equation. The particle size was determined from the diffraction peak (0 0 4) of the anatase phase of TiO_2 for angle 2θ = 37.79°, resulting in a crystallite size of 23 nm.

3.2. Electrochemical characterization TNM

The membranes were also evaluated electrochemically. Considering the previous observations in terms of embrittlement, morphology and light absorption, the TNM with t_{a1} = 1 h were preferred for the electrochemical and photoelectrochemical experiments. In the electrochemical evaluation of TNM on ITO as support through CV (Fig. 6b) the first impression is a different behaviour compared to the classic electrochemical response of NTs supported on Ti foil [29,30]. The loss of the capacitance at lower potential values is sharply decreased which might be attributed to the ohmic contact between the membranes and the ITO substrate [31,32]. However, the potential scan shows the typical signal for the photogenerated charge carriers under the UV irradiation where an increase of current density is observed. Thus, an electron charge transfer to the ITO is possible despite the loss of capacitance for these electrodes, suggesting that these membranes can be used for electrochemical applications [33].

If the polarization decreases to potentials lower than −0.4 V vs NHE, the evolution of H_2 takes place. The linear sweep voltammograms shown in Fig. 6c denote a similar behaviour to those observed in the CV. Here, a potential shoulder is developed at near 0.27 V vs NHE that might be attributed to possible trap states as observed by other authors [34].

It is also observed in the CVs a potential shift and widening of the signal, possibly due to the faster scan rate. Again, the photocurrent increase occurs with the UV light irradiation regardless of the presence of MeOH. However, the well-known current-doubling effect is observed, with an onset potential of −0.3 V vs NHE. In the distant zone of the charge carrier separation potential an increase of the photo-current is observed, with the maximum difference obtained being 42.76 mA cm^{-2} for acid profile and 63.85 mA cm^{-2} for the methanol oxidation (Fig. 6d).

3.3. Characterization Pt-Ru/TNM

The TNM modified with the Pt-Ru electrocatalyst were evaluated by physicochemical and photoelectrochemical studies. It was observed that the electrocatalyst was dispersed throughout the anodized surface, as evidenced by the SEM images when mapping the surface, revealing the homogeneous distribution of Pt-Ru on the surface modified with catalyst (Fig. 7a). The composition is fundamentally Ti, O, Pt, Ru and F. (Fig. 7b) and as evidenced by the EDS plot the catalyst is suitably supported on the membrane.

The electrochemical responses of the electrode in the presence and absence of irradiation are shown in Fig. 8. The typical NTs-TiO_2 response (Fig. 8a) is observed where for a wide range of anode potentials there are no electrochemical responses other than in the low potentials domain where a negative peak is developed which is usually associated with the adsorption of H^+ ions from the electrolyte. Under irradiation it was observed an increase in the current density in the same potential range for both bare TNM and Pt-Ru/TNM.

Pt-Ru/TNM shows a reduction wave at a potential of 0.2 V vs NHE followed by a second occurring at −0.2 V vs NHE can be seen in the CV, which can be attributed to the reduction of Pt the adsorption of hydrogen, accompanied by their anodic counterparts. When analysing the results of Fig. 8a, it is evident that the electrochemical response of the nanotubes differs before and after the modification with the electrocatalyst. The signals from these CVs correspond to the characteristic responses of Pt, and the modified support with the electrocatalyst is evidenced. However, the dramatic increase expected in current density (j) due to the electrooxidation of MeOH over the Pt-Ru electrocatalyst surface is not observed, this situation might arise because of the differences in conductivity mechanisms of the support (TNM), since in nanostructured semiconductors an electron gradient operates instead of classic metallic electron conduction. In more detail, the irradiated TNM separates charge (e^-/h^+ pairs), the electrons at the closest distance to the collecting substrate (ITO) are transferred to the outer circuit and the vacancies will oxidize the MeOH in the solution which in turn increases *j*. Nevertheless, the contribution of Pt-Ru to the electrooxidation of MeOH, $j_{ox\text{-}MeOH}$ takes place as an oxidation wave near 0.2 V vs NHE and

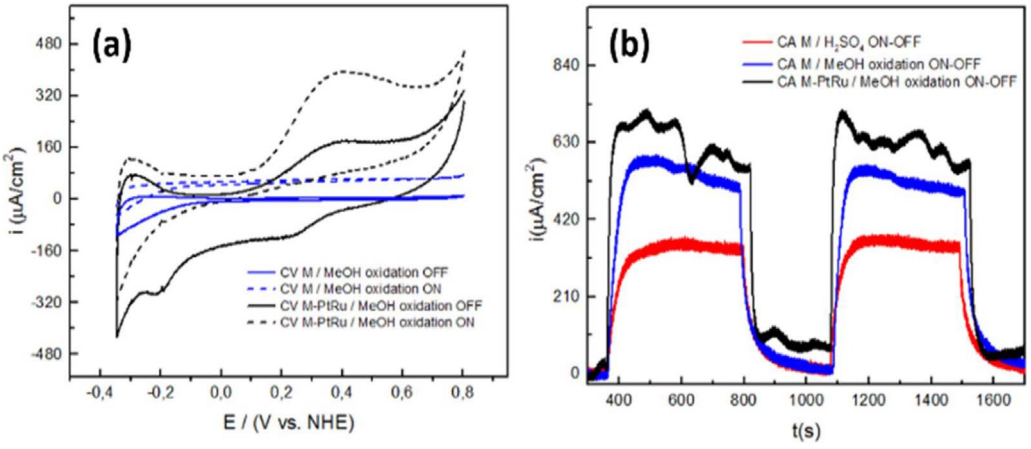

Fig. 8. Electrochemical characterization Pt-Ru/TNM a) CV methanol oxidation TNM and Pt-Ru/TNM ON-OFF. b) chronoamperogram, all in 0.5 M H_2SO_4 and 0.5 M MeOH/0.5 M H_2SO_4.

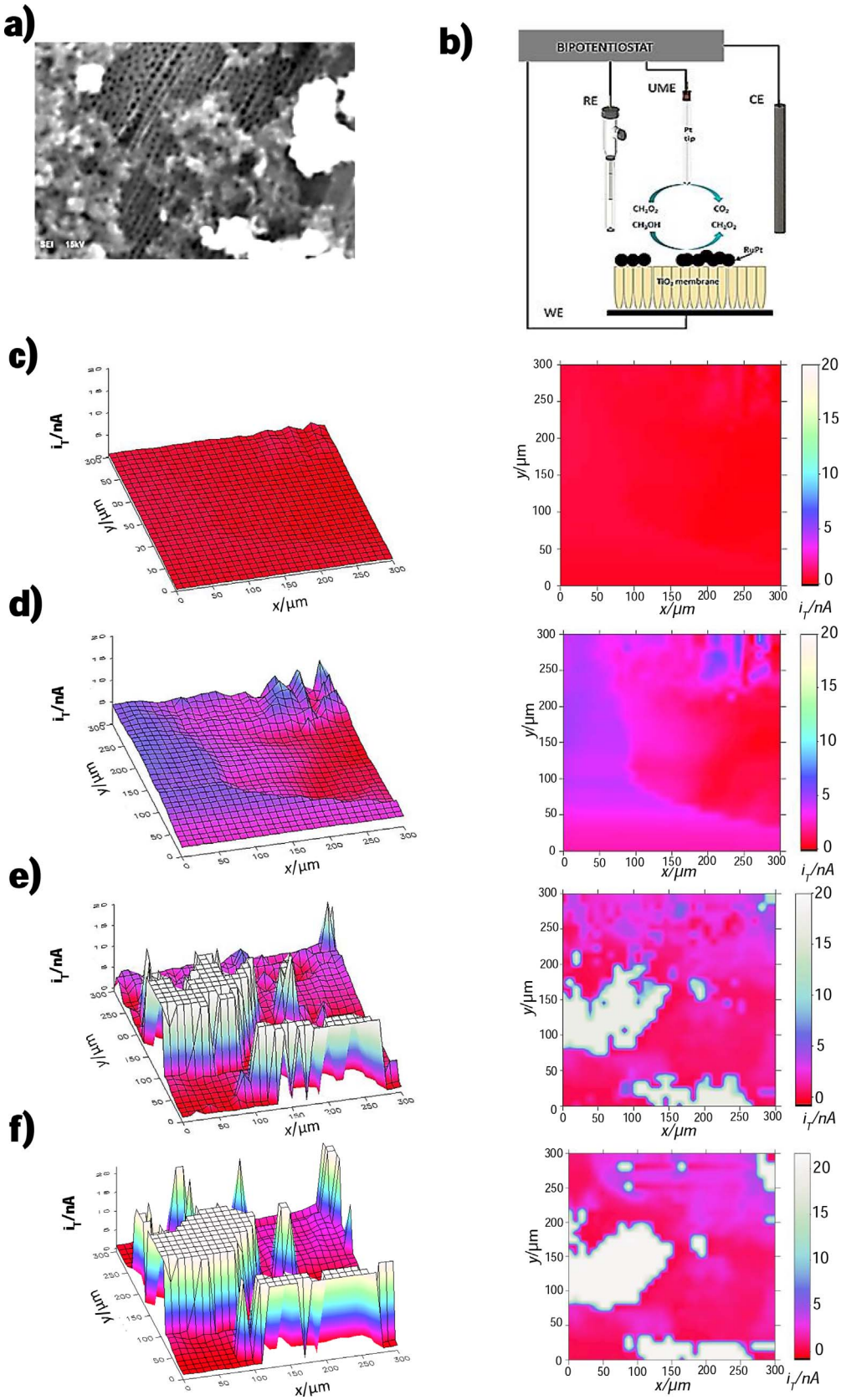

Fig. 9. a) Distribution of Pt-Ru catalyst on the surface of TNM. b) SECM experimental representation and SECM images obtained of the TNM using 0.5 M methanol/0.5 M H_2SO_4 c) without ultraviolet light (d) with ultraviolet light, (e) with deposited Pt-Ru nanoparticules and without ultraviolet light and (f) with deposited Pt-Ru nanoparticules and ultraviolet light on an area of 300 × 300 µm, 0.6 V of tip potential, 25 µm diameter Pt UME, with increments of 10 µm.

is more intense under UV irradiation.

The sudden electro-oxidative rise of *j* addressed to the fast kinetics of MeOH electro-oxidation over a Pt-Ru surface did not occurred. This might be explained in part by a slow charge transfer reaction between the electrocatalyst and the TNM. Either the electrons do not successfully reach the substrate (ITO), or a very small quantity is injected to the outer circuit, which increases slightly *j*, as it was observed in our experiment. Then this reveals the importance of the interfacial contact

between the electrocatalyst and its support (ohmic contact) as well as the intrinsic conductivity of this material, suggesting that such properties should also be tailored for a better performance.

The oxidation of methanol by chronoamperometry was also evaluated (Fig. 8b) at a potential of 0.2 V corresponding to the oxidation potential of the fuel, an aspect of fundamental interest for the future application of the electrodes as photoanodes in the methanol oxidation in the microfluidic fuel cells. The well-known current doubling effect was observed, with the maximum difference obtained being 100 μA cm^{-2} for the methanolic oxidation. Again, it was observed that the current generated with the Pt-Ru/TNM describes a non-constant value neither under darkness either under illumination, which suggests that the electron injection faces some events diminishing the evolution of *j*. However, the UV irradiated Pt-Ru/TNM electrode injects the photogenerated current which implies that the surface of the electrode is not blocked by the presence of the electrocatalyst; an important feature to be considered in photoelectrochemical applications.

The performance of electrodes was evaluated also by Scanning Electrochemical Microscopy, with and without Pt-Ru nanoparticles and under ultraviolet light and darkness (Fig. 9). As expected, some part of the surface of the nanotubes is obstructed by the presence of the catalyst dispersed in Nafion (Fig. 9a), which decreases the photocatalytic response of the material in a certain way to a stimulus with UV light. Fig. 9c shows the evaluation of the TiO_2 membrane in the presence of 0.5 M methanol in acid medium and without applying ultraviolet light, where a great change of current over the surface was not observed, because the membrane does not oxidize the methanol without UV light so that formic acid is not generated, and consequently not detected by the Pt UME. When UV is irradiated, a slight increase in current of 4.5 nA (Fig. 9d) is observed due to the photo-generated charge carriers. When Pt-Ru nanoparticles are applied to the surface of the membrane in darkness (Fig. 9e), there is an increase in current across the analysed surface area (300 × 300 μm) with zones (white colour) where a maximum current of 20 nA, increasing to 23 pA in some areas (white area) when UV is irradiated (Fig. 9f).

The illuminated Pt-Ru/TNM showed an interesting behaviour aroused from the interaction between the photocatalytic effect from the TNM and the Pt-Ru, where the current increases sharply in some areas while others do not present the same gain. The latter could be understood as electrocatalyst ink agglomeration or even obstruction by Nafion in local excess, since the TNM show a more regular response surface overriding an ohmic contact problem (TNM-ITO). More interestingly, this approach demonstrates indirectly the oxidizing action of photo-generated holes on MeOH by re-oxidizing the partially oxidized products, which can only be active when a recombination is overcome by effective electron collection on the TNM substrate due to the polarization. It is very interesting that the $j_{ox\text{-}MeOH}$ seems to be more dramatic, in contrast to our observations in the CA experiment.

Therefore, since the nature of the molecule investigated in both experiments are different (in CA it was directly MeOH, while in SECM is formic acid) it is possible to understand that the electron collection makes the difference in both. The deposition method for the electrocatalyst is also not so favourable for this system and reveals its impact in power generating applications. Then, the importance of increasing the internal conductivity in electron collection of the TNM is again demonstrated for which further experimentation and tuning of electrical properties of these materials should be considered prior to their incorporation into power generating systems.

4. Conclusions

In this work, it was confirmed the suitability of transfer and use of the TNM as substrate. The physicochemical characterization showed that crystallinity and composition of the samples are greatly determined by anodization and annealing processes. The electrochemical results demonstrated the importance of the internal conductivity of the support, which plays a major role in the performance of fuel cells. An improvement of this property accounts for an enhanced response in photocatalytic applications. The change in approach for the evaluation of MeOH photo/electrooxidation through the SECM setup allowed defining the contributions in current density between Pt-Ru electrocatalyst and TNM.

While these observations suggest the TNM as a promising photocatalyst support in devices that might profit from synergistic interaction of light stimulation and electrocatalytic modification; further experimentation is required to understand and improve conductivity issues with the electron collecting substrate.

Acknowledgements

The authors thank the Mexican Council for Science and Technology (CONACYT) for financial support through project LN-2017 280485, SENER 246079 and JADR thanks to PRODEP for Postdoctoral fellowship.

Appendix A. Supplementary data

Supplementary data associated with this article can be found, in the online version, at http://dx.doi.org/10.1016/j.apcatb.2017.09.019.

References

[1] Y.H. Lu, J. Li, Y.F. Tao, L.F. Hu, J. Alloys Compd. 679 (2016) 202–212.
[2] X. Jia, R. Dai, D. Lian, S. Han, H. Song, Appl. Surf. Sci. 392 (2017) 268–276.
[3] Z. Xu, T. Wu, J. Shi, K. Teng, W. Wang, M. Ma, J. Li, X. Qian, C. Li, J. Fan, J. Membr. Sci. 520 (2016) 281–293.
[4] B. Wang, F. Condi de Godoi, S. Zheng, I.R. Gentle, C. Li, Powder Technol. 302 (2016) 426–433.
[5] M. Wang, J. Ioccozia, L. Sun, C. Lin, Z. Lin, Energy Environ. Sci. 7 (2014) 2182–2202.
[6] M. Segev-Bar, A. Landman, M. Nir-Shapira, G. Shuster, H. Haick, ACS Appl. Mater. Interfaces 5 (2013) 5531–5541.
[7] H. Zhang, W. Zhou, Y. Du, P. Yang, J. Xu, , Int. J. Hydrog. Energy 35 (2010) 13290–13297.
[8] J. Ju, Y. Shi, D. Wu, Powder Technol. 230 (2012) 252–256.
[9] L. Xing, J. Jia, Y. Wang, B. Zhang, S. Dong, Int J. Hydrog. Energy 35 (2010) 12169–12173.
[10] W. Zhang, B. Li, H. Ma, L. Zhang, Y. Guan, Y. Zhang, X. Zhang, P. Jing, S. Yue, ACS Appl. Mater. Interfaces 8 (2016) 21465–21471.
[11] M. Segev-Bar, A. Landman, M. Nir-Shapira, G. Shuster, H. Haick, ACS Appl. Mater. Interfaces 5 (2013) 5531–5541.
[12] U. Gulzar, S. Goriparti, E. Miele, T. Li, G. Maidecchi, A. Toma, F. De Angelis, C. Capiglia, R.P. Zaccaria, J. Mater. Chem. A 4 (2016) 16771–16800.
[13] Y. Xiang, S. Lu, S.P. Jiang, Chem. Soc. Rev. 41 (2012) 7291–7321.
[14] Q. Hu, J. Liao, B. Zou, H. Wang, C. Chen, , J. Mater. Chem. A 4 (2016) 16801–16804.
[15] J.A. Díaz-Real, E. Ortiz-Ortega, M.P. Gurrola, J. Ledesma-Garcia, L.G. Arriaga, Electrochim. Acta 206 (2016) 388–399.
[16] S.P. Albu, A. Ghicov, J.M. Macak, R. Hahn, P. Schmuki, Nano Lett. 7 (2007) 1286–1289.
[17] F.D. Hardcastle, J. Ark Acad. Sci. 65 (2011) 43–48.
[18] Z. He, W. Que, Y. He, J. Hu, J. Chen, H.M.A. Javed, Y. Ji, X. Li, D. Fei, Ceram. Int. 39 (2013) 5545–5552.
[19] R. Asahi, T. Morikawa, Scince 293 (2001) 269–271.
[20] D. Monllor-Satoca, T. Lana-Villarreal, R. Gómez, Langmuir 27 (2011) 15312–15321.
[21] T.C. Jagadale, S.P. Takale, J. Phys. Chem. C 112 (2008) 14595–14602.
[22] N.C. Saha, H.G. Tompkins, J. Appl. Phys. 72 (1992) 3072.
[23] J.C. Yu, Wingkei Jiaguo, Lizhi Zitao, Chem. Mater. 14 (2002) 3808–3816.
[24] H.O. Finklea, Semiconductor Electrodes, Elsevier, Amsterdam, 1988, p. 520.
[25] R. Asahi, T. Morikawa, Science 293 (2001) 269–271.
[26] A.K. Rumaiz, J.C. Woicik, E. Cockayne, H.Y. Lin, G.H. Jaffari, S.I. Shah, Appl. Phys. Lett. 95 (2010) 262111.
[27] H. Park, W.R. Kim, H.T. Jeong, J.J. Lee, H.G. Kim, W.Y. Choi, Sol. Energy Mater. Sol. Cells 95 (2011) 184–189.
[28] P. Acevedo-Pena, F. Gonzalez, G. González, I. González, , Phys. Chem. Chem. Phys. 16 (2014) 26213–26220.
[29] M. Jankulovska, T. Berger, S.S. Wong, R. Gómez, T. Lana-Villarreal, Chem. Phys. Chem. 13 (2012) 3008–3017.
[30] H. Zhou, Y. Zhang, J. Phys. Chem. C 118 (2014) 5626–5636.
[31] G. Abadias, A.S. Gago, N. Alonso-Vante, Surf. Coat. Technol. 205 (2011) S265–S270.
[32] C. Montero-Ocampo, A. Gago, Environ. Sci. Pollut. Res. 19 (2012) 3751–3762.
[33] S. Miraghaei, F. Ashrafizadeh, Electrochem. Solid State Lett. 14 (2011) K8–K11.
[34] T. Frelink, W. Visscher, J.A.R. Veen, , J. Electroanal. Chem. 382 (1995) 65–72.